Inorganic Chemistry

Article

pubs.acs.org/IC

# Using High Pressure to Prepare Polymorphs of the $Ba_2Co_{1-x}Zn_xS_3$ ($0 \leq x \leq 1.0$) Compounds

Francesco Mezzadri,[†] Edmondo Gilioli,[‡] Gianluca Calestani,[†,‡] Andrea Migliori,[§] Mark R. Harrison,[∥] David A. Headspith,[∥] and M. Grazia Francesconi*[,∥]

[†]Dipartimento di Chimica GIAF, Universita' di Parma, Italy

[‡]Istituto CNR IMM sez. di Bologna, Italy

[§]LAMEL, CNR Bologna, Italy

[∥]Department of Chemistry, University of Hull, United Kingdom

Supporting Information

**ABSTRACT:** In this work, high pressure was used as a tool to induce structural transition and prepare metastable polymorphs of ternary sulfides. Structural transformations under high pressure of compounds belonging to the $Ba_2Co_{1-x}Zn_xS_3$ ($0 \leq x \leq 1.0$) series were studied using X-ray diffraction and electron microscopy. All members of the $Ba_2Co_{1-x}Zn_xS_3$ series show the $Ba_2CoS_3$-type one-dimensional structure, but, after heating under pressure, the $Ba_2CoS_3$ compound ($x = 0$) separates into BaS and the two-dimensional $BaCoS_{2-\delta}$ ($\delta \approx 0$), while $Ba_2Co_{1-x}Zn_xS_3$ compounds with $x \geq 0.25$ maintain their one-dimensional features but rearrange into polymorphs showing the $Ba_2MnS_3$-type structure. All structural transformations can be linked to shortening in interchain metal−metal distances caused by the high pressure, and the role of the zinc in preventing loss of one-dimensionality is discussed.

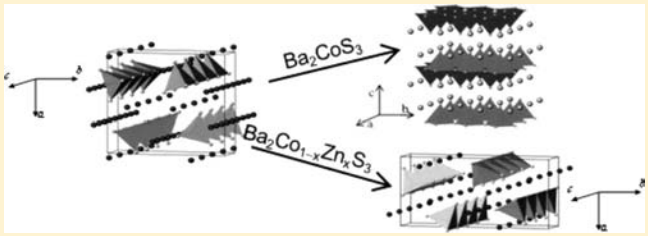


## INTRODUCTION

We exploited high pressure to prepare a series of new polymorphs within the $Ba_2Co_{1-x}Zn_xS_3$ ($0 \leq x \leq 1$) series and investigate the stability of their one-dimensional structure. The characterization of one-dimensional materials is usually welcome, as these systems have often been considered as a link between polymers or linear inorganic complexes and solid-state materials.[1] Furthermore, one-dimensional compounds are currently the object of renewed interest, due to their potential to form inorganic nanotubes and/or nanowires, without the use of templates or capping agents.

As well as chemical cationic and anionic substitutions, high pressure can be used as a tool for tuning the structure and properties of inorganic materials by varying interatomic distances and oxidation and coordination numbers, while observing changes in physical properties. The advantage of using high pressure on known materials to modify their structure and physical properties is that all the changes can be related to the changes in bond distances in a more straightforward manner than is possible with chemical routes, which always involve changes in composition and outer electron configuration of the ions.[2,3]

Sulfides are a class of relatively underexplored compounds compared to oxides, due, in part, to the greater experimental requirements for the synthesis of non-oxide materials but also to the enormous interest constantly devoted to the chemistry of oxides. However, with progress in preparation methods, the investigation of non-oxide materials has gained pace, fueled by the interesting and often unique physical properties they reveal.

The higher polarizability of the sulfide ion, relative to the oxide ion, ensures that sulfides are in general less ionic than oxides, and therefore, low-dimensional structures are encountered more frequently in sulfides.

One group of compounds, investigated for their quasi-one-dimensional magnetic structures, is the $Ba_2MS_3$ (M = Mn, Fe, Co, Zn, Cd, Hg) series.

Two families of structurally similar sulfides show this 213 stoichiometry: $Ba_2MS_3$ with M = Mn, Hg, Cd and $Ba_2MS_3$ with M = Fe, Co, Zn (Figure 1). Both $Ba_2MS_3$ families show one-dimensional chains of corner-linked M-S tetrahedra interleaved by $Ba^{2+}$ cations and two crystallographically different sites for $Ba^{2+}$. However, $Ba_2MS_3$ (M = Fe, Co, Zn) show the $K_2CuCl_3$-type structure, while $Ba_2MS_3$ (M = Mn, Hg, Cd) show the $K_2AgI_3$-type structure. A full description of the two structures and their similarities and differences is reported in the discussion of this paper.

$Ba_2MnS_3$ is insulating with a room temperature resistivity of $10^2$−$10^3$ Ω cm.[4] The resistivity of $Ba_2CoS_3$ is much lower at $\sim 10^{-1}$ Ω cm and thermopower measurements were indicative of metal-like conduction.[5] An investigation into $Ba_2FeS_3$ suggests limited electron delocalization. The high resistivity

**Received:** August 18, 2011
**Published:** December 16, 2011

   dx.doi.org/10.1021/ic201773e | *Inorg. Chem.* 2012, 51, 397−404

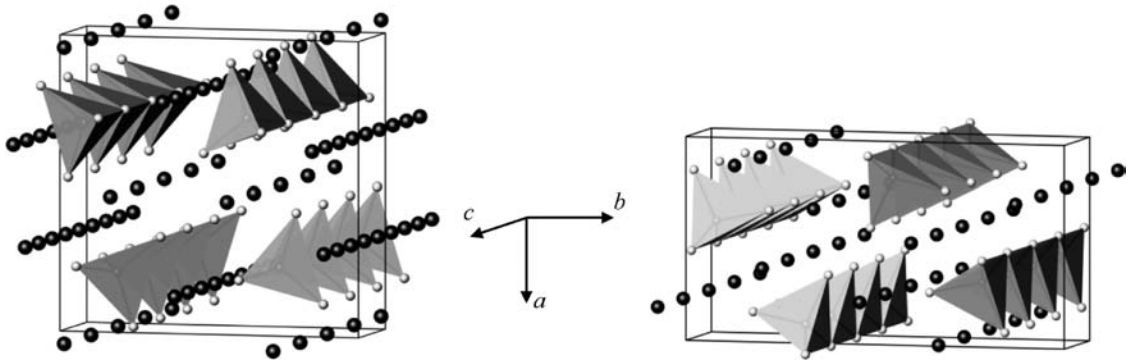


**Figure 1.** Structure of (a) $Ba_2MS_3$ (M = Zn, Co, Fe) and (b) $Ba_2MS_3$ (M = Mn, Hg, Cd). The dark and light gray spheres represent the barium and sulfur, respectively. The gray polyhedra are transition-metal-centered.

($10^4$ Ω cm), the effective magnetic moment of 5.29 $\mu_B$, and Mössbauer spectroscopy suggest that iron is present as $Fe^{2+}$.[6]

$Ba_2ZnS_3$ was first synthesized by Schnering and Hoppe in 1961 who found an orthorhombic unit cell of space group 62, *Pnma*, with parameters of $a$ = 12.05 Å, $b$ = 12.65 Å, and $c$ = 4.21 Å (no standard deviations were quoted).[7] $Ba_2CoS_3$ was first synthesized by Hong and Steinfink in a 1972 investigation into Ba−Fe−S phases, and was found to be isostructural to $Ba_2FeS_3$ and $Ba_2ZnS_3$.[8] An investigation into the magnetic susceptibilities of $Ba_2FeS_3$, $Ba_2CoS_3$, and $Ba_2MnS_3$ showed features consistent with quasi-one-dimensional antiferromagnetic short-range ordering.[9] Intrachain interactions, $J$, of −20, −15, and −12 K (in good agreement with value of −12.3(5) K previously reported for $Ba_2MnS_3$ and $Ba_2MnSe_3$)[10] were found for $Ba_2FeS_3$, $Ba_2CoS_3$, and $Ba_2MnS_3$. Long range magnetic ordering was found for all three compounds at 4.2 K due to interchain interactions.[9] The magnetic susceptibility of $Ba_2CoS_3$ has been reinvestigated, and the data again showed a broad peak indicative of one-dimensional magnetic ordering but also a transition to long-range order, at 46 K.[11,12] Interestingly, $Ba_2CoS_3$ shows negative magnetoresistance ∼ −1.7% in a 7 T field at 10 K, which is higher than that of the only other one-dimensional sulfide, $BaV_{0.8}Ti_{0.2}S_3$, so far reported to show negative MR.[5] Recently, it was reported that this negative magnetoresistance can be increased up to 9% via partial isovalent substitution of $Co^{2+}$ with the diamagnetic $Zn^{2+}$.[13]

In this work, we exploited high pressure to prepare a series of polymorphs of compounds belonging to the $Ba_2Co_{1-x}Zn_xS_3$ ($0 \le x \le 1$) series. For $x$ = 0.0, $Ba_2CoS_3$ separates into BaS and $BaCoS_{2-\delta}$ ($\delta \approx 0.0$), the two-dimensional sulfide with five-coordinated $Co^{2+}$ first reported by Snyder et al.,[14] even though a shift in the $Co^{2+}$ position from the 4e site in the *P4/nmm* is observed in this case. When $Zn^{2+}$ is partially substituted for $Co^{2+}$ ($x \ge 0.25$), monodimensionality and tetrahedral coordination of the transition metals are maintained and a structural transition to the $Ba_2MnS_3$-type structure takes place, giving new polymorphs of the $Ba_2Co_{1-x}Zn_xS_3$ ($0 \le x \le 1$) series.

## EXPERIMENTAL SECTION

The room pressure $Ba_2Co_{1-x}Zn_xS_3$ ($x$ = 0.0, 0.1, 0.2, 0.5, 1.0) series was prepared via solid−gas reaction between stoichiometric amounts of zinc oxide, barium carbonate, and cobalt and a $CS_2$ vapor carried by $N_2$ gas. Reactions were carried out at 1000 °C for 20 h followed by slow cooling, as described in previous publications.[13] Carbon disulfide is a liquid with a low vapor pressure. If nitrogen gas is bubbled through liquid $CS_2$, the gas acts as a carrier and a vapor of $N_2/CS_2$ can be passed through a tubular furnace. The nitrogen gas was first passed through concentrated sulfuric acid in order to remove any moisture and then through a Dreschel bottle containing liquid $CS_2$, which was in turn connected to the silica work tube of the furnace. Nitrogen gas was used to flush the system of air before the reaction was started, and to remove $CS_2$ once the reaction was completed. The downstream end of the silica tube was connected to another Dreschel bottle containing paraffin oil, which sealed the system from the air and acted as a postreaction scrubber, thus reducing the release.

Heating under HP was carried out using a multianvil apparatus. Polycrystalline $Ba_2Co_{1-x}Zn_xS_3$ samples were encapsulated into Pt foils and placed into a Walker-type module. The pressure was increased up to 60 kbars at a rate of 1 bar/min, then the capsule was heated up to 950 °C at a rate of 50°C/min. After 2 h in these conditions, the sample was cooled down to room temperature by switching off the heater. The pressure was finally slowly released at 0.4 bar/min.

Powder X-ray diffraction (PXRD) was carried out using a Thermo Electron ARL X'tra diffractometer equipped with a Si(Li) solid state detector and $CuK_\alpha$ radiation. Diffraction patterns were collected in the 15−70° 2$\theta$ range, with 0.02 step and counting times ranging from 1 to 5 s.

Single crystal X-ray diffraction was carried out using a Bruker APEX II diffractometer equipped with a CCD area detector by using graphite monochromatized Mo $K_\alpha$ radiation. Structure solution was performed using the Sir2004 program,[15] while refinements were carried out using Shelx97.[16]

Transmission electron microscopy (TEM) measurements were performed using a Philips TECNAI F20 instrument operating at 200 kV. The specimens were prepared by grinding the powder in isopropyl alcohol and evaporating the suspension on a copper grid covered with a holey carbon film.

## RESULTS

**Powder X-ray Diffraction(PXRD).** The PXRD patterns of $Ba_2CoS_3$, $Ba_2Co_{0.5}Zn_{0.5}S_3$ and $Ba_2ZnS_3$ before (RP) and after heating at high pressure (HP) are shown in Figures 2, 4, and 5.

The PXRD patterns in Figure 2 show that structural changes have occurred after heating $Ba_2CoS_3$ (RP). The peaks in the PXRD pattern of $Ba_2CoS_3$ heated under pressure were indexed using the structure of $BaCoS_{2-\delta}$[14,17,18] as a model for the main phase, and of BaS for the secondary phase. More unidentified impurities are present. $Ba_2CoS_3$ (*Pnam*, $a$ = 12.000(1) Å, $b$ = 12.470(1) Å, and $c$ = 4.205(2) Å) displays the one-dimensional $K_2CuCl_3$-type structure, whereas $BaCoS_{2-\delta}$ displays the two-dimensional $KCoO_2$-type structure (Figure 3). It appears that high pressure promotes the separation of $Ba_2CoS_3$ into BaS and $BaCoS_{2-\delta}$.

Tetragonal $BaCoS_{2-\delta}$ is isostructural to $BaNiS_2$;[19] however, a decrease in symmetry to orthorhombic or monoclinic is observed when $\delta$ increases. It is a metastable compound prepared by heating the mixture of starting reagents above 850


dx.doi.org/10.1021/ic201773e | *Inorg. Chem.* 2012, 51, 397−404

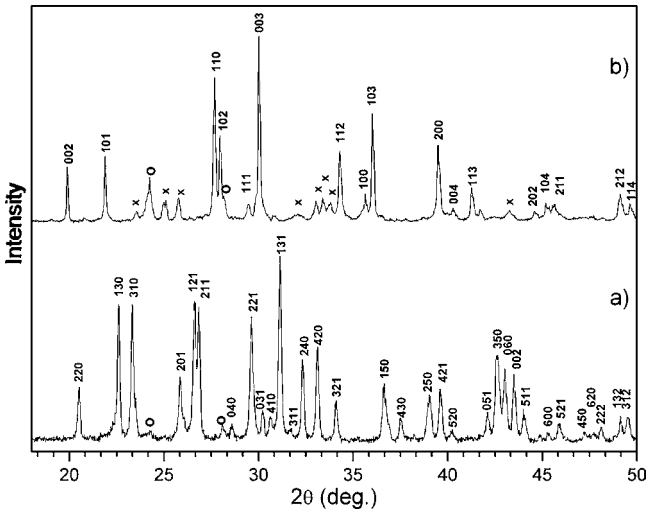


**Figure 2.** PXRD patterns of $Ba_2CoS_3$ before (a) and after (b) heating at 950 °C for two hours at $P$ = 60 kbars.

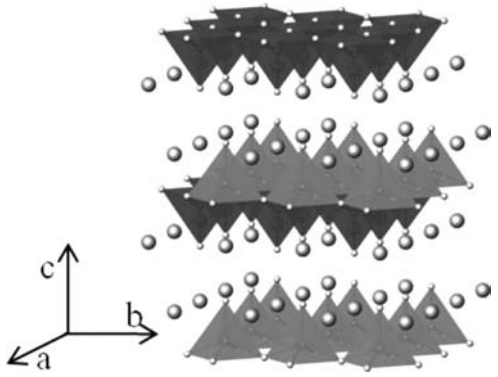


**Figure 3.** Structure of $BaCoS_{2-\delta}$. The larger gray spheres represent the $Ba^{2+}$ cations and the gray polyhedra represent the Co−S square pyramids.

°C and quenching it in an ice water bath. For a stoichiometric mixture of starting binary sulfides, BaS and CoS, a sulfur-deficient ($\delta \approx 0.2$) $BaCoS_{2-\delta}$ is obtained. The stoichiometric phase ($\delta \approx 0.0$) can be obtained only by using excess sulfur.[18] In our case, the PXRD pattern is consistent with a tetragonal symmetry and can be indexed on the basis of a *P*4/*nmm* unit cell with $a$ = 4.568(1) Å, $c$ = 8.942(2) Å), indicating a phase stoichiometry close to $BaCoS_2$. It can, therefore, be inferred that under high pressure $Ba_2CoS_3$ loses BaS stoichimetrically and transforms into $BaCoS_{2-\delta}$ with $\delta \approx 0.0$. A structural rearrangement takes place with cobalt expanding its coordination from tetrahedral to square pyramidal, the corner connectivity and one-dimension linear arrangement of the Co−S tetrahedra in $Ba_2CoS_3$ being lost in favor of edge connectivity and two-dimensional planar arrangement in $BaCoS_{2-\delta}$. Microanalysis on several crystallites confirms that the Ba:Co ratio is a 1:1 ratio.

Figures 4a,b and 5a,b show the PXRD pattern of $Ba_2Co_{0.5}Zn_{0.5}S_3$ and $Ba_2ZnS_3$, respectively, prepared at room pressure (RP) and after heating at high pressure (HP). A change in the structure of both compounds, as a consequence of high-pressure heating, is visible from the difference between the two PXRD patterns. The majority of peaks in the PXRD patterns of both $Ba_2Co_{0.5}Zn_{0.5}S_3$ (HP) and $Ba_2ZnS_3$ (HP) were indexed, using $Ba_2MnS_3$ as a model for the main phase and BaS

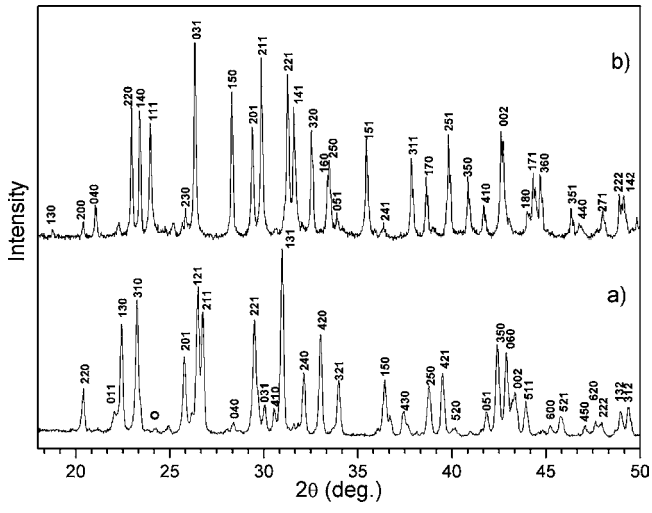


**Figure 4.** PXRD patterns of $Ba_2Co_{0.5}Zn_{0.5}S_3$ (a) before (RP) and (b) after (HP) heating at 950 °C for two hours at $P$ = 60 kbars.

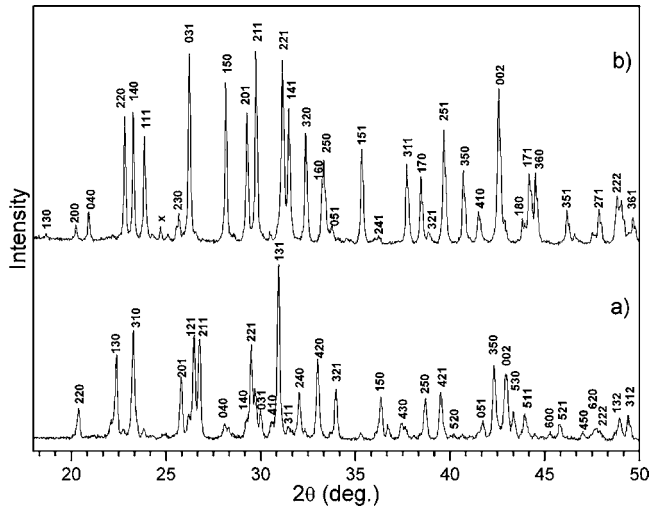


**Figure 5.** PXRD patterns of $Ba_2ZnS_3$ (a) before (RP) and (b) after (HP) heating at 950 °C for two hours at $P$ = 60 kbar.

for one of the secondary phases. Other unidentified phases are also present. $Ba_2Co_{0.5}Zn_{0.5}S_3$ and $Ba_2ZnS_3$ show the one-dimensional $K_2CuCl_3$-type structure, whereas $Ba_2MnS_3$ (*Pnma*; $a$ = 8.814(5) Å, $b$ = 4.302(2) Å, $c$ = 17.048(8) Å) shows the one-dimensional $K_2AgI_3$-type structure.[20] It appears that high pressure promotes a structural rearrangement from the $K_2CuCl_3$-type structure to the $K_2AgI_3$-type structure, thus giving new polymorphs of compounds in the $Ba_2Co_{1-x}Zn_xS_3$ series. Unlike in the case of the $x$ = 0 compound, $Ba_2CoS_3$, the one-dimensionality of the structure is maintained and the coordination of the transition metal remains tetrahedral. Microanalyses of several crystallites of selected $Ba_2Co_{1-x}Zn_xS_3$ samples, confirm that Ba:TM = 2:1.

Interestingly, reacting BaS with Co and S at 950 °C and 60 kbars and BaS with Zn and S under the same conditions gives $BaCoS_2$ + BaS and the $Ba_2ZnS_3$ polymorph with the $Ba_2MnS_3$-type structure, respectively.

**Single Crystal X-ray Diffraction.** X-ray diffraction was performed on selected single crystals from the samples of $Ba_2CoS_3$ (HP), $Ba_2Co_{0.4}Zn_{0.6}S_3$ (HP), and $Ba_2ZnS_3$ (HP). Unit cell and refinement parameters for $BaCoS_{2-\delta}$ and two of the


dx.doi.org/10.1021/ic201773e | *Inorg. Chem.* 2012, 51, 397−404

**Table 1. Unit Cell and Refinement Parameters for (a) $BaCoS_{2-\delta}$ ($\delta \approx 0.0$), (b) $Ba_2Co_{0.4}Zn_{0.6}S_3$, and (c) $Ba_2ZnS_3$ Obtained from Single Crystal X-ray Diffraction Data**

| (a) $BaCoS_2$ | (b) $Ba_2Co_{0.4}Zn_{0.6}S_3$ | (c) $Ba_2ZnS_3$ |
|---|---|---|
| $a = b = 4.564(1)$ $c = 8.938(1)$ Å | $a = 8.7577(8)$ $b = 16.9725(15)$ $c = 4.2528(4)$ Å | $a = 8.785(3)$ $b = 17.013(8)$ $c = 4.249(1)$ Å |
| $V = 186.18$ (1) | $V = 632.14(16)$ | $V = 635.05(4)$ |
| $\rho = 4.645$ | $\rho = 4.550$ | $\rho = 4.550$ |
| S.G. *P4/nmm* (129) | S.G. *Pnam* (62) | S.G. *Pnam* (62) |
| 2133 reflections of which 143 unique Max $2\theta = 52.87$ | 9300 reflections of which 929 unique Max $2\theta = 57.55$ | 1126 reflections, of which 1035 unique Max $2\theta = 59.97$ |
| Total number of l.s. parameters = 15 | Total number of l.s. parameters = 39 | Total number of l.s. parameters = 37 |
| $R_1 = 0.0114$ for 127 $F_o > 4\sigma$ and 0.143 for all 143 data | R1 = 0.0369 for 703 $F_o > 4\sigma$ (Fo) and 0.0560 for all 929 data | $R_1 = 0.0369$ for 681 $F_o > 4\sigma$ ($F_o$) and 0.0790 for all 1035 data |
| $wR_2 = 0.0263$ | $wR_2 = 0.0736$ | $wR_2 = 0.0638$ |
| GooF = 1.142 | GooF = 1.029 | GooF = 0.825 |
| Restrained GooF = 1.142 | Restrained GooF = 1.029 | Restrained GooF = 0.825 |

**Table 2. Atomic Coordinates for (a) $BaCoS_{2-\delta}$ ($\delta \approx 0.0$), (b) $Ba_2Co_{0.4}Zn_{0.6}S_3$, and (c) $Ba_2ZnS_3$ Obtained from Single Crystal X-Ray Diffraction Data**

(a) $BaCoS_2$

| ATOM | *x* | *y* | *z* | sof | $U_{11}$ | $U_{22}$ | $U_{33}$ | $U_{23}$ | $U_{13}$ | $U_{12}$ | $U_{eq}$ |
|---|---|---|---|---|---|---|---|---|---|---|---|
| Ba1 | 3/4 | −1/4 | 0.8019 (1) | 1 | 0.0172(2) | 0.0146(2) | 0.0146(2) | 0 | 0 | 0 | 0.0163(2) |
| Co1 | 3/4 | −1/4 | 0.4088(1) | 1 | 0.0199(3) | 0.0199(3) | 0.0170(5) | 0 | 0 | 0 | 0.0189(2) |
| S1 | 1/4 | 1/4 | 0.8493(2) | 1 | 0.0188(6) | 0.0188(6) | 0.0111(8) | 0 | 0 | 0 | 0.0162 (4) |
| S2 | 0.276(7) | −0.276(7) | 1/2 | 0.25 | 0.09(9) | 0.019(9) | 0.0223(11) | 0 | 0 | 0 | 0.020(6) |

$Ba_2Co_{0.4}Zn_{0.6}S_3$

| ATOM | *x* | *y* | *z* | sof | $U_{11}$ | $U_{22}$ | $U_{33}$ | $U_{23}$ | $U_{13}$ | $U_{12}$ | $U_{eq}$ |
|---|---|---|---|---|---|---|---|---|---|---|---|
| Ba1 | 0.2528(1) | 0.4555(1) | −1/4 | 1 | 0.0168(4) | 0.0131(4) | 0.0143(4) | 0 | 0 | −0.0006(3) | 0.0148(2) |
| Ba2 | 0.0808(1) | 0.2131(4) | 1/4 | 1 | 0.0145(4) | 0.0155(4) | 0.0134(4) | 0 | 0 | 0.0002(3) | 0.014(2) |
| Zn1 | −0.1333(2) | 0.3657(1) | −1/4 | 0.59(4) | 0.0120(9) | 0.0132(8) | 0.0186(9) | 0 | 0 | 0.0003(6) | 0.0146(6) |
| Co1 | −0.1333(2) | 0.3657(1) | −1/4 | 0.41(4) | 0.0120(9) | 0.0132(8) | 0.0186(9) | 0 | 0 | 0.0003(6) | 0.0146(6) |
| S1 | −0.1807(4) | 0.2294(2) | −1/4 | 1 | 0.0134(15) | 0.0134(15) | 0.0147(15) | 0 | 0 | 0.0002(11) | 0.0138(6) |
| S2 | −0.3707(3) | 0.4281(2) | −1/4 | 1 | 0.0123(16) | 0.0139(14) | 0.0146(16) | 0 | 0 | −0.0001(11) | 0.0136(6) |
| S3 | −0.0074(4) | 0.3977(2) | −3/4 | 1 | 0.0165(16) | 0.0158(14) | 0.0075(14) | 0 | 0 | −0.0003(12) | 0.0133(6) |

$Ba_2ZnS_3$

| ATOM | *x* | *y* | *z* | sof | $U_{11}$ | $U_{22}$ | $U_{33}$ | $U_{23}$ | $U_{13}$ | $U_{12}$ | $U_{eq}$ |
|---|---|---|---|---|---|---|---|---|---|---|---|
| Ba1 | 0.2540(1) | 0.4558(1) | −1/4 | 1 | 0.0054(3) | 0.0045(3) | 0.0055(4) | 0 | 0 | −0.0007(3) | 0.0052(2) |
| Ba2 | 0.0805(1) | 0.2133(1) | 1/4 | 1 | 0.004(3) | 0.0067(4) | 0.0055(4) | 0 | 0 | −0.0001(3) | 0.0055(2) |
| Zn1 | −0.1343(2) | 0.3656(1) | −1/4 | 1 | 0.0025(6) | 0.0043(7) | 0.0090(8) | 0 | 0 | −0.0006(6) | 0.0052(3) |
| S1 | −0.1809(3) | 0.2287(2) | −1/4 | 1 | 0.0021(12) | 0.0036(16) | 0.0082(16) | 0 | 0 | −0.0001(12) | 0.0046(7) |
| S2 | −0.3722(3) | 0.4281(2) | −1/4 | 1 | 0.0023(14) | 0.0034(14) | 0.0084(16) | 0 | 0 | −0.0011(11) | 0.0047(6) |
| S3 | −0.0057(3) | 0.3984(2) | −3/4 | 1 | 0.0049(13) | 0.0042(15) | 0.0042(16) | 0 | 0 | 0.0012(12) | 0.0044(6) |

high pressure polymorphs in the $Ba_2Co_{1-x}Zn_xS_3$ series are shown in Table 1, atomic coordinates in Table 2, and selected bond distances in Table 3.

For $BaCoS_{2-\delta}$, the S2 atom was initially refined in the 4e site. This resulted in atomic displacement parameters (a.d.p.s) significantly larger than the ones of S1, in agreement with previous determination.[14,17,18] Freeing the occupancy ratio for both sulfur anions did not result in any significant change, confirming the stoichiometry of the compound as close to $\delta \approx 0.0$. Taking into account that the large $U_{11}$ and $U_{22}$ values for S2 may be due to a displacement from the fourfold axis, S2 was then placed on the eightfold positions 8 h, with the occupancy fixed to one-half. The refinement converged for S2 located on a disordered position around the fourfold axis (Table 2a). The shifting of the S2 position normalizes the a.d.p.s and makes two of the four Co−S2 distances equivalent to the Co−S1 distances.

**Microscopy.** High resolution electron microscopy (HREM), electron diffraction (ED), and energy dispersive X-ray spectroscopy (EDX) analyses were performed on the $Ba_2CoS_3$, $Ba_2Co_{0.5}Zn_{0.5}S_3$, and $Ba_2ZnS_3$ samples after heating in high pressure (HP). EDX analyses on $Ba_2CoS_3$ (HP) were performed using several grains and confirmed the 1:1 Ba:Co ratio. The $BaCoS_{2-\delta}$-type unit cell from X-ray data was confirmed by the main reflections in the ED pattern (Figure 6). However, very weak satellites are associated with a diffuse streaking, indicating the doubling of the unit cell volume. By denoting as $a_T$ and $c_T$ the lattice parameters of the fundamental tetragonal cell, the new cell parameters, calculated from ED are $a \approx b = a_T\sqrt{2} = 6.4$ Å, $c = c_T = 8.9$ Å. A similar cell, associated with the *Cmma* space group, was previously used to refine both the stoichiometric and sulfur deficient structures.[14,18] However, it must be noted that the observed superstructure spots violate the C-centered extinction condition, suggesting the real structure to be primitive. Taking into account the very weak intensity of these satellite spots, the origin of this superstructure is probably attributed to the ordering of the shift of the S2


dx.doi.org/10.1021/ic201773e | *Inorg. Chem.* 2012, 51, 397−404

**Table 3. Selected Bond Distances for (a) $BaCoS_{2-\delta}$ ($\delta \approx 0.0$), (b) $Ba_2Co_{0.4}Zn_{0.6}S_3$, and (c) $Ba_2ZnS_3$ Obtained from Single Crystal X-ray Diffraction Data**

| (a) $BaCoS_2$ | | (b) $Ba_2Co_{0.4}Zn_{0.6}S_3$ | | $Ba_2ZnS_3$ | |
|---|---|---|---|---|---|
| Ba1−S1 | 3.118 (2) | Ba1−S1 | 3.192(3) | Ba1−S1 | 3.191(3) |
| Ba1−S1 | 3.255 (1) | Ba1−S2 | 3.081(2) | Ba1−S2 | 3.082(2) |
| Ba1−S1 | 3.255 (1) | Ba1−S2 | 3.081(2) | Ba1−S2 | 3.082(2) |
| Ba1−S1 | 3.255 (1) | Ba1−S2 | 3.268(2) | Ba1−S2 | 3.318(3) |
| Ba1−S1 | 3.255 (1) | Ba1−S3 | 3.268(2) | Ba1−S3 | 3.267(2) |
| Ba1−S2 | 3.46(2) | Ba1−S3 | 3.290(3) | Ba1−S3 | 3.267(2) |
| Ba1−S2 | 3.46(2) | Ba1−S3 | 3.330(3) | Ba1−S3 | 3.303(3) |
| Ba1−S2 | 3.46(2) | *Avg* | *3.216(2)* | *avg* | *3.216(3)* |
| Ba1−S2 | 3.46(2) | | | | |
| *avg* | *3.331(2)* | Ba2−S1 | 3.137(2) | Ba2−S1 | 3.139(2) |
| | | Ba2−S1 | 3.137(2) | Ba2−S1 | 3.139(2) |
| Co1−S1 | 2.307 (2) | Ba2−S1 | 3.137(2) | Ba2−S1 | 3.144(2) |
| Co1−S2 | 2.32 (3) | Ba2−S1 | 3.137(2) | Ba2−S1 | 3.144(2) |
| Co1−S2 | 2.32 (3) | Ba2−S2 | 3.227(3) | Ba2−S2 | 3.235(3) |
| Co1−S2 | 2.32 (3) | Ba2−S2 | 3.231(2) | Ba2−S2 | 3.235(3) |
| Co1−S2 | 2.32 (3) | Ba2−S3 | 3.231(2) | Ba2−S3 | 3.240(4) |
| *avg* | *2.317(3)* | *Avg* | *3.177(2)* | *avg* | *3.182(3)* |
| | | Zn1−S1 | 2.333(3) | Zn1−S1 | 2.364(3) |
| | | Zn1−S2 | 2.351(3) | Zn1−S2 | 2.344(3) |
| | | Zn1−S3 | 2.456(2) | Zn1−S3 | 2.470(2) |
| | | Zn1−S3 | 2.456(2) | Zn1−S3 | 2.470(2) |
| | | *Avg* | *2.404(3)* | *avg* | *2.412(3)* |
| Co1−Co1 | 3.619(6) | Zn1−Zn1 | 4.25(4) | Zn1−Zn1 | 4.25(2) |
| Co1−Co1 | 4.565(5) | Zn1−Zn1 | 5.57(5) | Zn1−Zn1 | 5.55(2) |
| | | Zn1−Zn1 | 5.90(4) | Zn1−Zn1 | 5.88(1) |

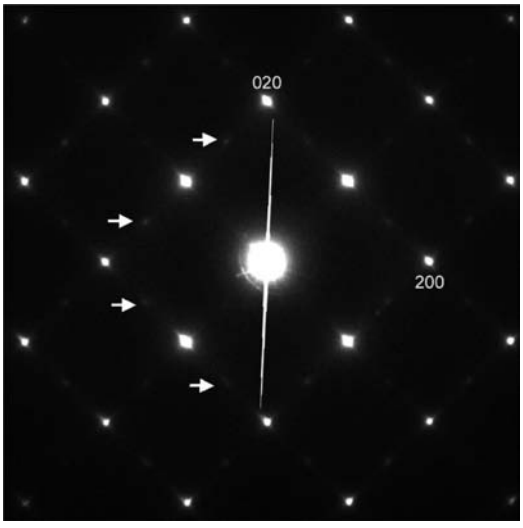


**Figure 6.** ED patterns of a $BaCoS_2$ grain taken in [001] zone axis and indexed on the basis of the tetragonal *P*4/*nmm* cell: very weak superlattice spots (indicated by arrows and associated to diffuse streaking) are observed.

anions from the 4e site, shown by single-crystal X-ray diffraction data.

EDX analyses performed on $Ba_2Co_{0.5}Zn_{0.5}S_3$ and $Ba_2ZnS_3$ samples confirmed a composition close to the nominal one, whereas ED and HREM confirmed the $Ba_2MnS_3$ type unit cell, as found via X-ray diffraction. A high-resolution electron microscopy (HREM) image of a $Ba_2Co_{0.5}Zn_{0.5}S_3$ sample is shown in Figure 7.

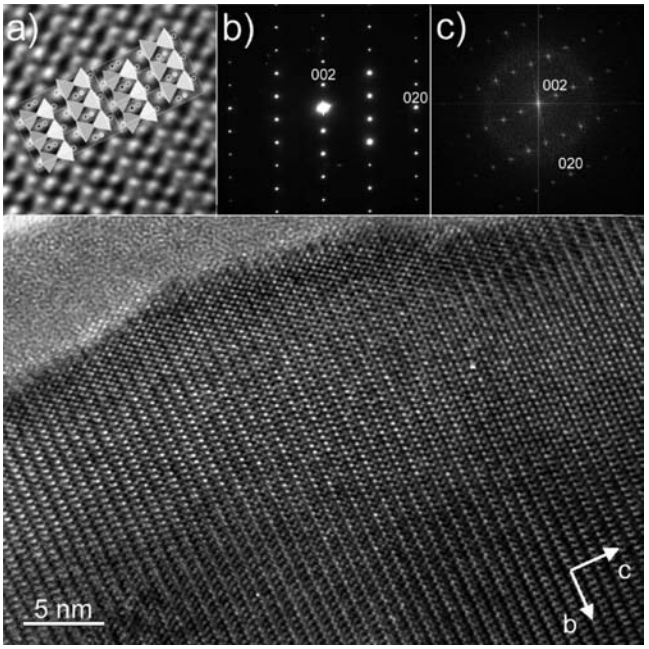


**Figure 7.** HREM image of a $Ba_2Co_{0.5}Zn_{0.5}S_3$ sample taken along the *a* axis; an enlargement of the image is shown in inset (a), compared with the structural model; the corresponding experimental ED pattern and the fast Fourier transform of the image are shown in insets (b) and (c), respectively.

**Discussion.** The $Ba_2MS_3$ sulfides with M = Fe, Co, Zn and M = Mn, Hg, Cd share the same stoichiometry and a number of structural similarities, mainly one-dimensional chains of corner linked M-S tetrahedral interleaved by $Ba^{2+}$ cations (Figure 1). These compounds can be split into two groups of isostructural materials. $Ba_2MS_3$ (M = Zn, Co, Fe) show the $K_2CuCl_3$-type structure, while $Ba_2MS_3$ (M = Mn, Hg, Cd) show the $K_2AgI_3$-type structure. In both cases, the corner sharing tetrahedra run along the shortest axis and both structures show two crystallographically independent barium sites with the barium coordinated to seven anions. These barium cations show monocapped trigonal prismatic coordination with the chalcogens, with the capping anion lying above the center of one of the rectangular faces of the prism. Shoemaker analyzed the differences between the $K_2CuCl_3$ and $K_2AgI_3$ structures,[21] and here, we adapt some of those concepts to the $Ba_2CoS_3$ (*Pnam*, 11.994(2) Å, 12.472(2) Å, 4.201(1) Å)[12] and $Ba_2MnS_3$ (*Pnma*, 8.814(5) Å, 4.302(2) Å, 17.0480(80) Å)[20] structures. In order to facilitate direct comparison between the compounds, $Ba_2MS_3$ (M = Mn, Fe, Hg, Cd) has been considered redefined in the space group *Pnam*, rather than *Pnma*, in which it were originally classified, by inverting the values of the *b* and *c* axes.

In both structure types, the monocapped trigonal prisms, centered on Ba(1), form chains of triangular face-sharing polyhedra running along the short axis, *c*. In line with the description by Shoemaker, the Ba(1) coordination can be extended to include an eighth anion.[21] This eighth anion can be taken as capping a second rectangular face of the prism, shown by the dashed lines in Figure 8a. It is these square-based pyramids that separate the $MX_4$ tetrahedra of the M-X chains in both type of structures. The square-based pyramids formed by


dx.doi.org/10.1021/ic201773e | *Inorg. Chem.* 2012, 51, 397−404

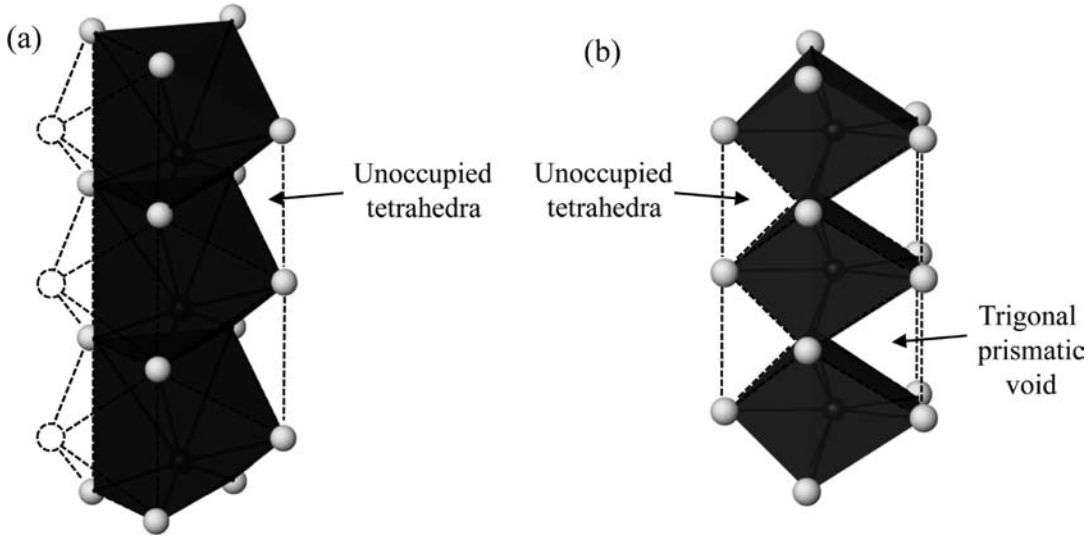


**Figure 8.** Representation of (a) the face sharing chains of Ba(1) centered polyhedra and (b) the edge sharing chains of Ba(2) centered polyhedra.

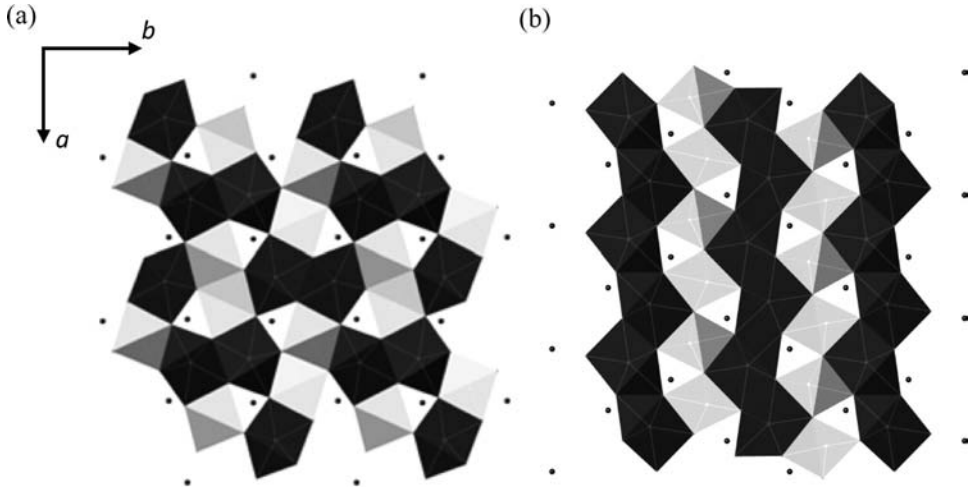


**Figure 9.** Representation of the (a) $Ba_2CoS_3$-type and (b) $Ba_2MnS_3$-type structures. The two crystallographically independent barium positions are represented at the center of the monocapped trigonal prisms in dark and light gray. The black spheres correspond with the transition metal site.

the original capping anion, to the right-hand side of the trigonal prismatic chains, also form tetrahedra of sulfide anions without a metal in the center.

The Ba(2) polyhedra form chains of edge sharing monocapped trigonal prisms along *c*, with the prism axis perpendicular to the *c*-axis. To the right of these chains of monocapped trigonal prisms, as represented in Figure 8b, is a trigonal prismatic void that also shares a face with the M-X chains. On the opposite side of this polyhedral chain, the capping anions give rise to another, corner-sharing, chain of unoccupied tetrahedra. It is reasonable to speculate that it is the presence of these voids that plays a role in the interconversion of the $Ba_2CoS_3$-type structure into the $Ba_2MnS_3$-type structure under high pressure.

The difference between the two structure types is the manner in which these Ba−S chains are arranged with respect to one another, which can be seen more clearly when observing projections down the structures down the [001] as shown in Figure 9. In $Ba_2MnS_3$, the $Ba(1)S_7$ polyhedra form corner-linked linear chains and the $Ba(2)S_7$ form edge-sharing linear chains. However, in $Ba_2CoS_3$ the $Ba(1)S_7$ and $Ba(2)S_7$ polyhedra both form face-sharing dimeric units. The $Ba(1)S_7$ dimeric units are isolated from one another, whereas the dimeric $Ba(2)S_7$ polyhedra are connected to four other $Ba(2)S_7$ dimeric units via corner linkages. This differing arrangement of the $BaS_7$ polyhedra for $Ba_2MnS_3$ and $Ba_2CoS_3$ results in a different arrangement of the $MS_4$ corner linked linear chains as shown in Figure 9. $Ba(1)S_7$ and $Ba(2)S_7$ polyhedra in $Ba_2MnS_3$ are surrounded by two and four Mn−S tetrahedral chains, respectively, while in $Ba_2CoS_3$, they are both surrounded by three Co−S tetrahedral chains.

Hull and Berastegui studied a series of alkaline-transition metal halides showing either the $Ba_2CoS_3$-type or the $Ba_2MnS_3$-type structure and found that the formation of one or the other is dictated by the ratio $r_A/r_M$ with A = transition metal and M = alkaline metal.[3] In particular, the $Ba_2CoS_3$-type structure is favored for the smaller values of the $r_A/r_M$ ratio. We calculated the $r_{M^{2+}}/r_{Ba^{2+}}$, with $M^{2+}$ = Mn, Co, Zn, Cd, Hg, for the $Ba_2MS_3$ family with the data available to date, and found that compounds with $r_{M^{2+}}/r_{Ba^{2+}} \leq 0.435$ exhibit the $Ba_2CoS_3$-type structure, whereas compounds with $r_{M^{2+}}/r_{Ba^{2+}} \leq 0.478$ exhibit the $Ba_2MnS_3$-type structure (Table 4).

All compounds belonging to the $Ba_2Co_{1-x}Zn_xS_3$ solid solution show the $Ba_2CoS_3$-type structure, but our results


dx.doi.org/10.1021/ic201773e | *Inorg. Chem.* 2012, 51, 397−404

**Table 4. $r_{M^{2+}}/r_{Ba^{2+}}$ Radius Ratios for $Ba_2CoS_3$-Type and $Ba_2MnS_3$-Type Structures**

| Compound $Ba_2MS_3$ | Radius of M (Å) | $r_{M^{2+}}/r_{Ba^{2+}}$ | Structure |
|---|---|---|---|
| $Ba_2CoS_3$ | 0.58 | 0.420 | $Ba_2CoS_3$-type |
| $Ba_2Co_{0.5}Zn_{0.5}S_3$ | 0.59 | 0.428 | $Ba_2CoS_3$-type |
| $Ba_2ZnS_3$ | 0.60 | 0.435 | $Ba_2CoS_3$-type |
| $Ba_2MnS_3$ | 0.66 (HS) | 0.478 | $Ba_2MnS_3$-type |
| $Ba_2CdS_3$ | 0.78 | 0.435 | $Ba_2MnS_3$-type |
| $Ba_2HgS_3$ | 0.96 | 0.700 | $Ba_2MnS_3$-type |

show that, after heating in high pressure, they turn into polymorphs with the $Ba_2MnS_3$-type structure. Considering that high pressure tends to change the distances and angles between atoms in a structure, we performed a comparison of bond lengths and angles between the (RP) and (HP) compounds. Comparison between Ba−S and M−S bond-length do not reveal significant differences between the two polymorphs. However, differences are observed between the M−M interchain distances, i.e., the distances between the transition metal at the center of M−S tetrahedra belonging to neighboring chains. In fact, the M−M interchain distances in $Ba_2CoS_3$ are 6.13(7) and 6.57(6),[12] but they are shorter in $Ba_2MnS_3$, namely, 5.457 and 5.9673.[22]

**Table 5. M−M Interchain Distances of Compounds with the $Ba_2CoS_3$-Type and $Ba_2MnS_3$-Type Structures**

| Compound $Ba_2MS_3$ | M−M interchain (Å) | Structure |
|---|---|---|
| $Ba_2ZnS_3$ RP | 6.17; 6.67[22] | $Ba_2CoS_3$-type |
| $Ba_2Co_{0.5}Zn_{0.5}S_3$ RP | 6.14(3); 6.61(3)[13] | $Ba_2CoS_3$-type |
| $Ba_2CoS_3$ RP | 6.13(7); 6.57(6)[12] | $Ba_2CoS_3$-type |
| $Ba_2Co_{0.4}Zn_{0.6}S_3$ HP | 5.57(5); 5.90(4) [this work] | $Ba_2MnS_3$-type |
| $Ba_2ZnS_3$ HP | 5.55(2); 5.88(1) [this work] | $Ba_2MnS_3$-type |
| $Ba_2MnS_3$ RP | 5.46; 5.97[22] | $Ba_2MnS_3$-type |

**Table 6. Selected Distances and Angles for Compounds of the (RP) $Ba_2Co_{1-x}Zn_xS_3$ Series with $x \geq 0$**

| $x$ | 0.0 | 0.25 | 0.5 | 0.75 |
|---|---|---|---|---|
| | | bond lengths | | |
| M-S(1) | 2.330(3) | 2.31(3) | 2.32(3) | 2.35(3) |
| M-S(2) | 2.317(3) | 2.33(3) | 2.32(3) | 2.32(3) |
| M-S(3) | 2.427(2) | 2.430(15) | 2.45(2) | 2.46(2) |
| M-M intrachain | 4.205(2) | 4.2064(10) | 4.2059(10) | 4.2099(10) |
| M-M interchain | 6.153(3), 6.582(4) | 6.60(3), 6.14(3) | 6.61(3), 6.14(3) | 6.63(3), 6.14(3) |
| | | angles | | |
| S(1)-M-S(2) | 111.71(10) | 110.7(3) | 110.7(3) | 110.4(3) |
| S(1)-M-S(3) | 105.81(8) | 106.4(3) | 106.7(3) | 105.7(3) |
| S(2)-M-S(3) | 106.72(11) | 106.7(3) | 107.2(3) | 108.7(3) |
| S(3)-M-S(3) | 120.11(8) | 119.85(15) | 118.40(15) | 117.5(2) |

Table 6 shows a comparison between the M−M interchain distances of compounds with the $Ba_2CoS_3$-type and the $Ba_2MnS_3$-type structures.

The data in Table 5 show that the average M−M interchain distances for compounds showing the $Ba_2CoS_3$-type structure are 6.15 Å and 6.62 Å, whereas for compounds showing the $Ba_2MnS_3$-type structure, they are 5.53 Å and 5.92 Å. The critical M−M value is probably around 6 Å.

From these data, it can be inferred that the compression exercised by high pressure compressing the materials with $Ba_2CoS_3$-type structure is felt on the *ac* plane, perpendicular to the *b* axis, along which run the chains of tetrahedral M−S. The unoccupied tetrahedral around the Ba(1)-S and Ba(2)-S chains probably provides empty space for the structure to rearrange.

Another important result is that $Ba_2CoS_3$ (RP) transforms into $BaCoS_{2-\delta}$, whereas all the compounds belonging to the Zn-substituted series $Ba_2Co_{1-x}Zn_xS_3$ (RP) transform into polymorphs with the $Ba_2MnS_3$-type structure. This indicates that the presence of $Zn^{2+}$ partially substituted on the $Co^{2+}$ site is the determining factor to obtain polymorphs. $Zn^{2+}$ shows a slightly larger ionic radius ($r$ = 0.60 Å) than $Co^{2+}$ ($r$ = 0.58 Å) in tetrahedral coordination; however, this small difference may be the determining factor in the formation of the (HP) polymorphs.[23] Using the $r_{M^{2+}}/r_{Ba^{2+}}$ ratio, it can be argued that for $r_{M^{2+}}/r_{Ba^{2+}} \leq 0.420$ either the $Ba_2CoS_3$-type or the $Ba_2MnS_3$-type structures are not stable anymore and the 112 structure is formed, with consequent loss of BaS. Furthermore, by observing the changes in bond lengths and angles introduced by the substitution of $Zn^{2+}$ in $Ba_2CoS_3$ (RP), it can be noticed that the bond distances do not change significantly and neither do the angles, moving from $x = 0$ to $x > 0$. However, $Ba_2CoS_3$ was found to show very distorted Co−S tetrahedra, as can be seen from the values of the angles,[24] but the substitution of $Zn^{2+}$ for $Co^{2+}$ seems to favor all angles approaching109.47°, i.e., the angle of the perfect tetrahedron and, therefore, a tendency to remove the distortion. The changing of the angles with increasing Zn content is particularly visible in the variation of the S(3)−M−S(3) angle (Table 6). This may indicate that, under high pressure, the tetrahedral coordination of $Co^{2+}$ in the $x = 0$ compound, $Ba_2CoS_3$, is too distorted to be maintained but the substitution of $Zn^{2+}$ removes enough distortion for the tetrahedral coordination to survive. However, the $Ba_2CoS_3$-type structure is transformed into the $Ba_2MnS_3$-type structure due to the shortening of the M−M interchain distances.

## CONCLUSIONS

We have reacted selected members of the $Ba_2Co_{1-x}Zn_xS_3$ ($0 \leq x \leq 1.0$) series at 950 °C and 60 kbars pressure. All the starting materials show the $Ba_2CoS_3$-type structure. However, for $x = 0$ $Ba_2CoS_3$ separates into BaS and $BaCoS_{2-\delta}$, whereas for $x > 0$, a series of polymorphs showing the $Ba_2MnS_3$-type structure are obtained. The formation of the $Ba_2MnS_3$-type polymorphs implies retention of one-dimensionality and tetrahedral coordination of the transition metal, whereas the formation of $BaCoS_{2-\delta}$ implies loss of one-dimensionality in favor of bidimensionality and loss of the tetrahedral coordination of the metal in favor of square pyramidal coordination. It is argued that the partial $Co^{2+}/Zn^{2+}$ substitution is the crucial factor in the formation of the one-dimensional polymorphs over $BaCoS_{2-\delta}$, which is determined by the high pressure shortening the M-M interchain distance.

## ASSOCIATED CONTENT

### Supporting Information

CIF file. This material is available free of charge via the Internet at http://pubs.acs.org.

## AUTHOR INFORMATION

### Corresponding Author

*E-mail m.g.francesconi@hull.ac.uk.

## ■ ACKNOWLEDGMENTS

M. R. Harrison and M. G. Francesconi thank the EPSRC for the award of a research grant (EP/E029469). M. G. Francesconi also acknowledges the RSC for the award of a travel grant (08 10 621). We wish to acknowledge the use of the Chemical Database Service at Daresbury.

## ■ REFERENCES

(1) De Jongh, L. J.; Miedema, A. R. *Adv. Phys.* **1974**, *23*, 1−260.
(2) Badding, J. V.; Meng, J. F.; Polvani, D. A. *Chem. Mater.* **1998**, *10*, 2889−2894.
(3) Hull, S.; Berastegui, P. *J. Solid State Chem.* **2004**, *177*, 3156−3173.
(4) Greaney, M. A.; Ramanujachary, K. V.; Teweldemedhin, Z.; Greenblatt, M. *J. Solid State Chem.* **1993**, *107*, 554−562.
(5) Baikie, T.; Hardy, V.; Maignan, A.; Francesconi, M. G. *Chem. Commun.* **2005**, 5077−5079.
(6) Reiff, W. M.; Grey, I. E.; Fan, A.; Eliezer, Z.; Steinfink, H. *J. Solid State Chem.* **1975**, *13*, 32−40.
(7) Schnering, v. H. G.; Hoppe, R. *Z. Anorg. Allg. Chem.* **1961**, *312*, 99−109.
(8) Hong, H. Y.; Steinfin., H *J. Solid State Chem.* **1972**, *5*, 93−&.
(9) Nakayama, N.; Kosuge, K.; Kachi, S.; Shinjo, T.; Takada, T. *Abstr. Pap. Am. Chem. Soc.* **1979**, 58−58.
(10) Grey, I. E.; Steinfink, H. *Inorg. Chem.* **1971**, *10*, 691−696.
(11) Baikie, T.; Maignan, A.; Francesconi, M. G. *Chem. Commun.* **2004**, 836−837.
(12) Headspith, D. A.; Battle, P. D.; Francesconi, M. G. *J. Solid State Chem.* **2007**, *180*, 2859−2863.
(13) Harrison, M. R.; Hardy, V.; Maignan, A.; Francesconi, M. G. *Chem. Commun.* **2009**, 2214−2216.
(14) Snyder, G. J.; Gelabert, M. C.; Disalvo, F. J. *J. Solid State Chem.* **1994**, *113*, 355−361.
(15) Burla, M. C. C., R.; Camalli, M.; Carrozzini, B.; Cascarano, G. L.; De Caro, L.; Giacovazzo, C.; Polidori, G.; Spagna, R. *J. Appl. Crystallogr.* **2005**, *38*, 381.
(16) Sheldrick, G. M. 1993.
(17) Baenziger, N. C.; Grout, L.; Martinson, L. S.; Schweitzer, J. W. *Acta Crystallogr., Sect. C* **1994**, *50*, 1375−1377.
(18) Gelabert, M. C.; Brese, N. E.; DiSalvo, F. J.; Jobic, S.; Deniard, P.; Brec, R. *J. Solid State Chem.* **1996**, *127*, 211−221.
(19) Steinfink, I. E. G. a. H. *J. Am. Chem. Soc.* **1970**, *92*, 5093.
(20) Grey, I. E.; Steinfin., H *Inorg. Chem.* **1971**, *10*, 691−&.
(21) Shoemaker, C. B. *Z. Kristallogr.* **1973**, *137*, 225−239.
(22) Fletcher, D. A.; McMeeking, R. F.; Parkin, D. *J. Chem. Inf. Comput. Sci.* **1996**, *36*, 746−749.
(23) Shannon, R. D. *Acta Crystallogr., Sect. A* **1976**, *32*, 751−756.
(24) Barnes, A. D. J.; Baikie, T.; Hardy, V.; Lepetit, M. B.; Maignan, A.; Young, N. A.; Francesconi, M. G. *J. Mater. Chem.* **2006**, *16*, 3489−3502.